The Immersed Boundary Method for incompressible fluid–structure interaction

David M. McQueen, Charles S. Peskin *, Luoding Zhu

Courant Institute of Mathematical Sciences, New York University, 251 Mercer Street, New York, NY 10012, USA

Abstract

In this paper the Immersed Boundary Method is presented, with some recent developments. The method is used to analyze fluid–structure interaction problems. Different aspects of the method are illustrated by applying it to blood flow in the heart and a flapping filament (flag-in-wind) problem.

Keywords: Immersed Boundary Method; Fluid–structure interaction; Cardiac fluid dynamics; Flapping filament; Flag in wind; Computational fluid dynamics; Incompressible elasticity; Heart valves

1. Introduction

In the study of fluid–structure interaction, it is useful to think of the structure as a part of the fluid where additional forces are applied, and where additional mass may be localized. In this paper, we consider the case of a viscous incompressible fluid that interacts with an immersed structure that is made of an incompressible viscoelastic material. To keep things as simple as possible, we assume that the viscosity is Newtonian and uniform throughout the system. This restriction can certainly be removed, but we shall not address that complication here. The mass density of the ambient fluid is also assumed to be uniform, but the structure is allowed to have a nonuniform mass density which may be greater or lower than that of the fluid.

Instead of separating the system into its two components coupled by boundary conditions, as is conventionally done, we use the incompressible Navier–Stokes equations, with a nonuniform mass density and an applied elastic force density, to describe the coupled motion of the hydroelastic system in a unified way. In order to do this, however, we need to supplement the Navier–Stokes equations by a Lagrangian description of the elastic material, from which the elastic force density and the nonuniform mass density that appear in the Navier–Stokes equations may be calculated. Moreover, we need a mathematical apparatus to translate in either direction between Lagrangian quantities and the corresponding Eulerian quantities. This apparatus is conveniently provided by the Dirac delta function.

The equations of motion that result from this point of view directly motivate a numerical method known as the "Immersed Boundary Method" [1–5]. This name emphasizes an important feature of the method: that it can handle not only immersed elastic structures that displace a finite volume, but also immersed elastic boundaries like heart valve leaflets (for which the method was originally designed), insect wings, sails, and parachutes, all of which may be idealized as surfaces which, despite having zero volume, nevertheless apply finite forces to the fluid in which they are immersed. Clearly, the Dirac delta function is particularly well suited to this situation.

2. Equations of motion

As described in Section 1, we use an Eulerian description of the system as a whole (fluid + structure) supplemented by a Lagrangian description of the structure. The independent variables of the Eulerian description are the Cartesian coordinates $\boldsymbol{x}$ and the time t, and the independent variables of the Lagrangian description are curvilinear material coordinates q, r, s and again the time t. The Eulerian description of the system as a whole involves the velocity field $\boldsymbol{u}(\boldsymbol{x}, t)$, the hydrostatic pressure field $p(\boldsymbol{x}, t)$, the mass density $\rho(\boldsymbol{x}, t)$ and the Eulerian elastic force density $\boldsymbol{f}(\boldsymbol{x}, t)$. The Lagrangian description of the immersed elastic material involves its configuration $\boldsymbol{X}(q, r, s, t)$, its Lagrangian

* Corresponding author. Tel.: +1 (212) 998-3126; Fax: +1 (212) 995-4121; E-mail: peskin@cims.nyu.edu

elastic force density $\boldsymbol{F}(q, r, s, t)$, and its Lagrangian additional mass density $M(q, r, s)$, the integral of which over any chunk of the material gives the mass of that chunk minus the mass of the fluid displaced. Since both the mass and volume of any such chunk of the immersed elastic material are conserved, M is independent of time. Note that $M = 0$ in the case of a neutrally buoyant structure, and that M will be negative at any material point for which the mass density of the immersed elastic material is less than that of the ambient fluid. To complete the Lagrangian description of the elastic material, we need to specify the elastic potential energy functional, $E[\boldsymbol{X}]$, which is used in the calculation of the elastic forces from the configuration $\boldsymbol{X}(\,,\,,\,,t)$ at any given time. The mass density ρ_0 of the ambient fluid and the viscosity μ of the system as a whole are constant parameters. With this notation, our equations of motion read as follows:

$$\rho(\boldsymbol{x}, t)\left(\frac{\partial \boldsymbol{u}}{\partial t} + \boldsymbol{u}\cdot\nabla\boldsymbol{u}\right) + \nabla p = \mu\nabla^2\boldsymbol{u} + \boldsymbol{f}(\boldsymbol{x}, t) \tag{1}$$

$$\nabla\cdot\boldsymbol{u} = 0 \tag{2}$$

$$\boldsymbol{f}(\boldsymbol{x}, t) = \int \boldsymbol{F}(q, r, s, t)\,\delta\left(\boldsymbol{x} - \boldsymbol{X}(q, r, s, t)\right)\,\mathrm{d}q\,\mathrm{d}r\,\mathrm{d}s \tag{3}$$

$$\rho(\boldsymbol{x}, t) = \rho_0 + \int M(q, r, s)\,\delta\left(\boldsymbol{x} - \boldsymbol{X}(q, r, s, t)\right)\,\mathrm{d}q\,\mathrm{d}r\,\mathrm{d}s \tag{4}$$

$$\begin{aligned}\frac{\partial \boldsymbol{X}}{\partial t}(q, r, s, t) &= \boldsymbol{u}\left(\boldsymbol{X}(q, r, s, t), t\right)\\ &= \int \boldsymbol{u}(\boldsymbol{x}, t)\,\delta\left(\boldsymbol{x} - \boldsymbol{X}(q, r, s, t)\right)\,\mathrm{d}\boldsymbol{x}\end{aligned} \tag{5}$$

$$\boldsymbol{F} = -\frac{\partial E}{\partial \boldsymbol{X}} \tag{6}$$

These equations (without the viscous term) can be formally derived from the principle of least action, see [6] for details. Here we just give an informal discussion of their meaning.

Eqs. (1) and (2) are the familiar Navier–Stokes equations of a viscous incompressible fluid, with a variable mass density $\rho(\boldsymbol{x}, t)$ and an applied force density $\boldsymbol{f}(\boldsymbol{x}, t)$. Although it may be unconventional to use these equations in the case of an elastic material, one should recall that in the derivation of the incompressible Navier–Stokes equations the only ingredients are Newton's laws of motion, incompressibility, and a particular form of the stress tensor. It follows that the incompressible Navier–Stokes equations are applicable to *any* incompressible material, provided that appropriate allowance is made for the particular stress-tensor of the material, which may, of course, be different from that of a fluid. Here, the applied force density $\boldsymbol{f}(\boldsymbol{x}, t)$, the divergence of the elastic stress tensor, plays that role.

Note that Eq. (1) also involves the non-uniform mass density $\rho(\boldsymbol{x}, t)$. Since the fluid and the structure are both incompressible, it must be the case that $\rho(\boldsymbol{x}, t)$ at any given material point is independent of time, i.e., that $\mathrm{D}\rho/\mathrm{D}t = 0$, where $\mathrm{D}/\mathrm{D}t$ is the material derivative: $\partial/\partial t + \boldsymbol{u}\cdot\nabla$. This constraint is implicit in Eqs. (4) and (5); it does not have to be imposed separately.

Eqs. (3) and (4) provide conversions from the Lagrangian force and mass densities $\boldsymbol{F}(q, r, s, t)$ and $M(q, r, s)$ to the corresponding Eulerian force and mass densities, $\boldsymbol{f}(\boldsymbol{x}, t)$ and $\rho(\boldsymbol{x}, t)$, respectively. The relationship between corresponding densities is *not* that their values are the same at corresponding points, but rather that their integrals over corresponding regions are equal. One can confirm that this is satisfied in our case by integrating Eq. (3) or Eq. (4) over some arbitrary region of space, changing the order of the integrals on the right-hand side, and noting that the integral of the Dirac delta function yields 1 or 0 depending on whether or not the domain of integration includes the point $\boldsymbol{x} = \boldsymbol{X}(q, r, s, t)$.

It is important to note that Eqs. (3) and (4) still make sense in the special case that the immersed elastic structure takes the form of a surface instead of displacing any volume. In the case of such a structure (like a sail or parachute canopy), we need only drop one of the three Lagrangian coordinates q, r, s so that Eqs. (3) and (4) become

$$\boldsymbol{f}(\boldsymbol{x}, t) = \int \boldsymbol{F}(r, s, t)\,\delta\left(\boldsymbol{x} - \boldsymbol{X}(r, s, t)\right)\,\mathrm{d}r\,\mathrm{d}s \tag{7}$$

$$\rho(\boldsymbol{x}, t) = \rho_0 + \int M(r, s)\,\delta\left(\boldsymbol{x} - \boldsymbol{X}(r, s, t)\right)\,\mathrm{d}r\,\mathrm{d}s \tag{8}$$

In each of these equations, the Dirac delta function is still three-dimensional, but there are only two integrations to perform so the result is singular like a one-dimensional delta function. Again, the integral of $\boldsymbol{f}(\boldsymbol{x}, t)$ or $\rho(\boldsymbol{x}, t)$ over any finite three-dimensional region gives a finite result.

Eq. (5) states that the velocity of any material point of the structure may be found by evaluating the Eulerian velocity field $\boldsymbol{u}(\boldsymbol{x}, t)$ at the current location of that material point. This is essentially the definition of the Eulerian velocity field, but it also enforces the no-slip condition at the interface between the fluid and the structure, since we require that $\boldsymbol{u}$ be continuous. The second form of Eq. (5), in which the Dirac delta function appears, shows that the conversion from Eulerian to Lagrangian velocity can be expressed in a manner that resembles the conversions from Lagrangian to Eulerian force and mass densities, Eqs. (3) and (4). All of these conversions involve integral operators in which the Dirac delta function appears as a kernel. In Eq. (5), however, the integral is over the fixed Cartesian coordinates $\boldsymbol{x}$, whereas in Eqs. (3) and (4) the integrals are over the moving curvilinear material coordinates q, r, s.

Eq. (6) is shorthand for the statement that $\boldsymbol{F}$ is minus the Frechet derivative of E. That is, $\mathrm{d}E = -\int \boldsymbol{F}\cdot\mathrm{d}\boldsymbol{X}\,\mathrm{d}q\,\mathrm{d}r\,\mathrm{d}s$,

for any perturbation d$\boldsymbol{X}$, up to terms of higher order in d$\boldsymbol{X}$. This is essentially the principle of virtual work.

3. Numerical method

The Immersed Boundary Method is obtained by discretization of the above equations of motion. For details in the uniform density case, see [2–5]. The case of non-uniform mass density is similar, except that the Navier–Stokes solver involves the solution of difference equations with non-constant coefficients at each time step. Thus, Fourier transform methods are no longer applicable, and some iterative method such as multigrid must be used. An example of such a computation can be found in [7], and we report on another such example here.

4. Results

In this section, we present results of two different immersed boundary computations, illustrating different aspects of the method. The first is a computer simulation of the heart. It involves all aspects of the mathematical formulation mentioned above except that the density of the system is considered uniform. In particular, heart muscle is modeled as an anisotropic, incompressible, elastic material that is neutrally buoyant in blood, and the heart valve leaflets are modeled as massless fiber-reinforced elastic membranes. The elastic parameters of the heart muscle are time-dependent, which is what makes it possible for the model heart to beat.

The second computation presented here is a simulation of a laboratory experiment involving a flexible filament suspended in a flowing soap film with the upstream end of the filament held fixed. Because the fluid is in the form of a soap film, the whole problem is inherently two-dimensional, and the immersed boundary (the flexible filament) is one-dimensional. Filament mass, we have found, is an essential feature of the problem. Therefore, this computation illustrates those aspects of the Immersed Boundary Method that are concerned with non-uniform density.

The heart model [2,8] is shown in Figs. 1–3. It is made entirely of elastic and contractile fibers immersed in viscous incompressible fluid. The model includes the four cardiac chambers and all four valves; it also includes the great vessels to which the heart is connected. These great vessels of the model have blind ends but are equipped with sources and sinks that provide appropriate loads for the model heart. An external source/sink allows for changes in cardiac volume and also provides a convenient reference pressure. The specific form of the Immersed Boundary Method used for these computations is described in [5], see also [4]. Parameters, including the Reynolds number, are those of the human heart.

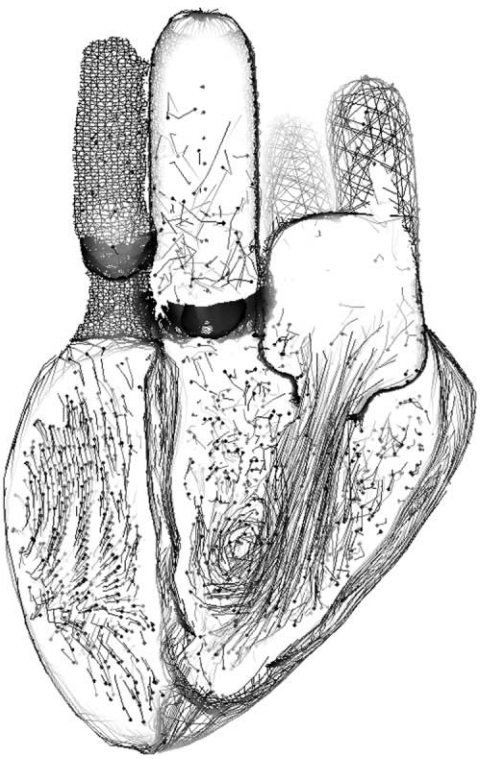

Fig. 1. Cutaway view of the three-dimensional heart model during ventricular filling. The heart is viewed from the front, so the left ventricle is on the right side of the figure and the right ventricle is on the left. Structures that appear above the ventricles are (from left to right in the figure) the main pulmonary artery (with closed pulmonic valve), the ascending aorta (with closed aortic valve), and the left atrium (with open mitral valve). Two pulmonary veins are visible behind and connecting to the left atrium. Fluid flow is shown in terms of streaklines: dots mark the current positions of blood particles, and tails attached to these dots show the trajectories of these particles over the recent past. Note the prominent vortex that was shed from the anterior leaflet of the mitral valve and has migrated down towards the apex of the left ventricle.

Figs. 1 and 2 show cutaway views of the heart in diastole from different perspectives. In Fig. 1 the clipping plane cuts through the mitral valve, the aortic valve, and the apex of the heart. Note the prominent vortex that was shed primarily from the anterior leaflet of the mitral valve and has then been convected towards the apex of the heart by the jet of left ventricular filling. In Fig. 2 the model heart has been turned so that the right ventricle faces the viewer. A large swirling vortex with an interesting 3D structure fills the relaxing right ventricular chamber. Fig. 3 shows the flow pattern of blood on the left side of the heart during ejection. Note the closed mitral valve, supported by papillary muscles and chordae tendineae, that prevents backflow into the left atrium, and the open aortic valve that allows the left ventricle to eject blood into the aorta.

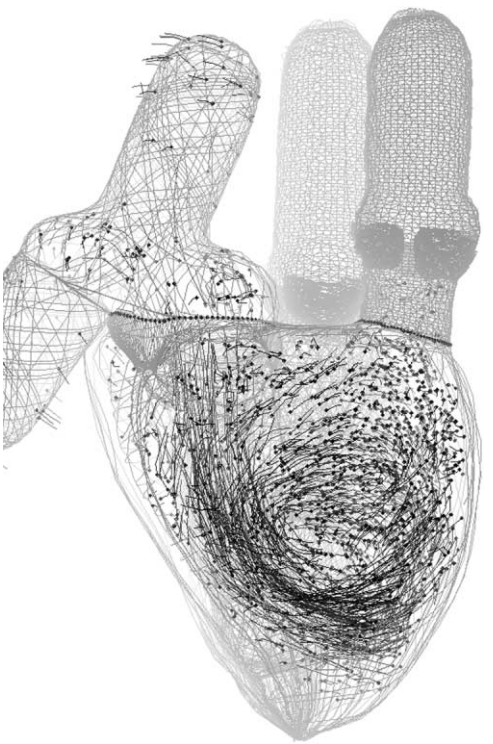

Fig. 2. Transparent view of the predicted flow pattern of right ventricular filling. The heart model has been turned so that the free wall of the right ventricle is in front. At the upper left in the figure, the superior vena cava and inferior vena cava join to form the right atrium. The open tricuspid valve is visible at the atrioventricular junction. Other structures seen above the ventricle are (from left to right in the figure) the ascending aorta and the main pulmonary artery. Note the flow pattern of the prominent vortex that seems to fill the entire right ventricle. There is a hint of 3D structure in the way that the flow comes down through the tricuspid valve in the foreground but swirls around the vortex core into the background behind that inflow jet.

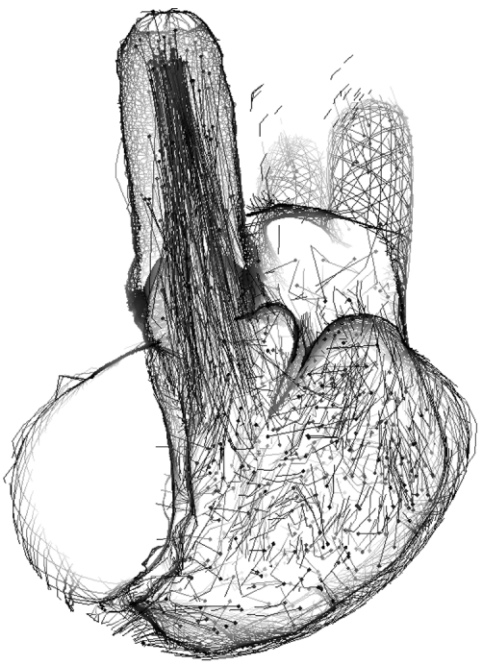

Fig. 3. The computed flow pattern of left ventricular ejection. Note the tension in the closed mitral valve and the jet of blood entering the ascending aorta through the open aortic valve.

It is our hope that this model will prove useful as a computer test chamber for the design of prosthetic cardiac valves. (For early studies of this kind in a two-dimensional left heart model, see [9–11].)

Computer simulation of a flapping filament in a flowing soap film is shown in Fig. 4. The filament, a flexible thread, is anchored at its upper end in a soap film which flows downwards under the influence of gravity, constrained by two vertical wires at the edges of the film. Air resistance flattens the velocity profile of the flowing soap film. This simulation is based on an experiment performed in the Courant Institute WetLab by Jun Zhang [12]. Zhang's key discovery is that under a range of conditions the filament exhibits bistable behavior. Its two stable states are: (1) a steady state in which the filament points straight downstream; or (2) a sustained oscillation in which the filament flaps like a flag in the wind and alternately sheds vortices of opposite sign creating a wake that resembles the Karman vortex street behind a cylinder. Either state is stable against small perturbations (hence the term 'bistable') but can be converted to the other state by a sufficiently large perturbation.

Our principal finding is that the flapping state requires filament mass. With a massless filament, the steady state in which the filament points straight downstream is globally stable. Fig. 4 shows a simulation in which the filament mass per unit length is twice that of the experimental filament (saturated with water), the extra mass being explained by a bulge in the soap film that forms around the thread as a consequence of surface tension, thus raising the effective filament mass. Although the Reynolds number of the computation (Re = 210) is lower than that of the laboratory experiment by two orders of magnitude, the results of the simulation are in good agreement with those of the experiment, including the observed flapping frequency of about 50 Hz.

5. Conclusions

The Immersed Boundary Method is a practical way to simulate fluid–structure interaction in the incompressible case. It can handle immersed elastic structures which displace finite volumes (like muscle), and also immersed

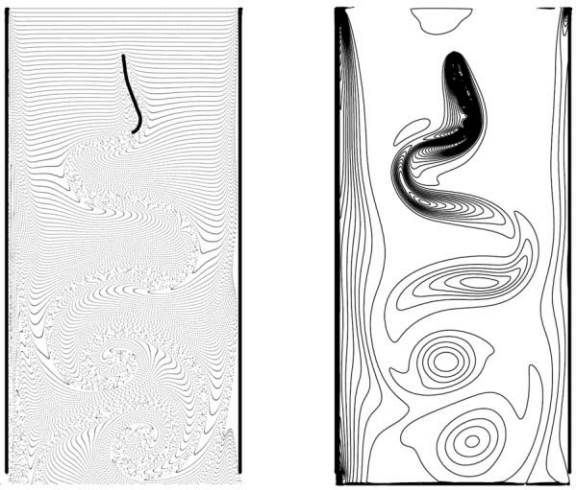

Fig. 4. Computer simulation of a flapping filament in a flowing soap film. Selected time step from a simulation showing sustained oscillation at about 50 Hz. Two different visualization techniques are used. The left panel of the figure shows the instantaneous positions of fluid markers created in bursts along the upper (inflow) boundary, as in a hydrogen bubble flow visualization. The right panel of the figure shows the corresponding vorticity contours. In both panels flow is from top to bottom (driven by gravity, working against air resistance) at an inflow velocity of 280 cm/s. The filament length is 3 cm, and the width of the channel is 8.5 cm. The Reynolds number of the computation (based on inflow velocity and filament length) is $\mathrm{Re} = 210$. The flapping filament sheds vortices of alternate sign which then form the sinuous wake seen in the figures.

elastic membranes (like sails, parachutes, and heart valve leaflets). Recent developments have extended the range of Reynolds numbers that the method can handle (up to and including that of the human heart), and have also made possible the simulation of immersed elastic structures which are not neutrally buoyant in the ambient fluid.

Acknowledgements

The authors are indebted to the National Science Foundation (USA) for support of this work under KDI research grant DMS-9980069. Computation was performed in part on the Cray T-90 computer at the San Diego Supercomputer Center under an allocation of resources MCA93S004P from the National Resource Allocation Committee.

References

[1] Peskin CS. Flow Patterns Around Heart Valves: A Digital Computer Method for Solving the Equations of Motion. Ph.D. Thesis, Albert Einstein College of Medicine, July, 1972, 211 pp. (available at http://www.umi.com/hp/Products/DisExpress.html, order number: 7230378)

[2] Peskin CS, McQueen DM. Fluid dynamics of the heart and its valves. In: Othmer HG, Adler FR, Lewis MA, Dallon JC (Eds), Case Studies in Mathematical Modeling: Ecology, Physiology, and Cell Biology. Englewood Cliffs NJ: Prentice-Hall, 1996, pp. 309–337.

[3] McQueen DM, Peskin CS. Shared-memory parallel vector implementation of the immersed boundary method for the computation of blood flow in the beating mammalian heart. J Supercomput 1997;11(3):213–236.

[4] Lai M-C, Peskin CS. An immersed boundary method with formal second order accuracy and reduced numerical viscosity. J Comput Phys 2000;160:705–719.

[5] McQueen DM, Peskin CS. Heart Simulation by an Immersed Boundary Method with Formal Second-Order Accuracy and Reduced Numerical Viscosity. ICTAM 2000 Proceedings, New York: Kluwer (in press).

[6] Peskin CS, McQueen DM. Computational biofluid dynamics. Contemp Math 1993;141:161–186.

[7] Fogelson AL, Zhu J. Implementation of a variable-density Immersed Boundary Method. Unpublished, http:/www.math.utah.edu/∼fogelson.

[8] McQueen DM, Peskin CS. A three-dimensional computer model of the human heart for studying cardiac fluid dynamics. Comput Graph 2000;34:56–60.

[9] McQueen DM, Peskin CS. Computer-assisted design of pivoting-disc prosthetic mitral valves. J Thorac Cardiovasc Surg 1983;86:126–135.

[10] McQueen DM, Peskin CS. Computer-assisted design of butterfly bileaflet valves for the mitral position. Scand J Thor Cardiovasc Surg 1985;19:139–148.

[11] McQueen DM, Peskin CS. Curved Butterfly Bileaflet Prosthetic Cardiac Valve. US Patent Number 5,026,391; June 25, 1991.

[12] Zhang J, Childress S, Libchaber A, Shelley M. Flexible filaments in a flowing soap film as a model for one-dimensional flags in a two-dimensional wind. Nature 2000;408:835.